A&A 400, 903–915 (2003)
DOI: 10.1051/0004-6361:20030004

Astronomy & Astrophysics

The ISOGAL field FC–01863+00035: Mid-IR interstellar extinction and stellar populations⋆,⋆⋆,⋆⋆⋆

B. W. Jiang[1,2,3], A. Omont[2], S. Ganesh[2,4], G. Simon[5], and F. Schuller[2]

[1] Department of Astronomy, Beijing Normal University, Beijing 100875, PR China
[2] Institut d'Astrophysique de Paris, CNRS, 98 bis Bd Arago, 75014 Paris, France
[3] National Astronomical Observatories, Chinese Academy of Sciences, Datun Rd. No.20(A), Beijing 100012, PR China (on leave)
[4] Physical Research Laboratory, Navarangpura, Ahmedabad 380009, India
[5] GEPI, Observatoire de Paris, 21 avenue de l'Observatoire, 75014 Paris, France

Received 18 July 2002 / Accepted 23 December 2002

Abstract. A $0.35^\circ \times 0.29^\circ$ field centered at $l = -18.63^\circ$, $b = 0.35^\circ$ was observed during the ISOGAL survey by ISOCAM imaging at 7 μm and 15 μm. 648 objects were detected and their brightness are measured. By combining with the DENIS data in the near-infrared J and K_S bands, one derives the extinction at 7 μm through $A_{K_S} - A_7 = 0.35(A_J - A_{K_S})$ which yields $A_7/A_V \sim 0.03$ from the near-IR extinction values of van de Hulst–Glass (Glass 1999). The extinction structure along the line of sight is then determined from the values of $J-K_S$ or K_S–[7] of the ISOGAL sources identified as RGB or early AGB stars with mild mass-loss. The distribution of A_V ranges from 0 to ∼45 and it reflects the concentration of the extinction in the spiral arms. Based on their locations in color-magnitude diagrams and a few cross-identifications with IRAS and MSX sources, the nature of objects is discussed in comparison with the case of a low extinction field in Baade's Window. Most of the objects are either AGB stars with moderate mass loss rate or luminous RGB stars. Some of them may be AGB stars with high mass loss rate. In addition, a few young stellar objects (YSOs) are present.

Key words. stars: AGB and post-AGB – stars: late-type – stars: mass loss – stars: pre-main sequence – ISM: dust, extinction – Galaxy: stellar content – Infrared: stars

1. Introduction

ISOGAL is an ISOCAM survey at 7 μm and 15 μm, at a spatial resolution in pixel-field-of-view of 6″ and sensitivity about 10 mJy, of about 16 deg^2, toward the Galactic plane mostly interior to $|l| = 30^\circ$ (Omont et al. 2003). About 200 fields observed are well spread in the inner bulge and in the Galactic disk. In combination with the DENIS data (Epchtein et al. 1997), the colors between 15 μm, 7 μm, K_S, J, I in the ISOGAL-DENIS catalogue (Schuller et al. 2003) allows a detailed study of cold stellar populations. For example, this survey shall result in a practically complete census of mass-losing AGB stars in the fields of the inner bulge and in some parts of the Galactic disk. The stars at the RGB tip may also be well characterized in the ISOGAL catalogue, as well as nearby or massive young stellar objects (YSOs). In addition to the study of cold stellar populations, another goal of ISOGAL is to study the Galactic structures in regions highly obscured through the inner Galaxy with a sensitivity and spatial resolution about two orders of magnitude better than IRAS.

FC–01863+00035 is one of the disk fields within the ISOGAL survey. In order to avoid strong sources saturating the ISOCAM detectors, an ISOGAL field is usually limited to a small $l \times b$ raster where no bright IRAS objects exist. The field FC–01863+00035 covers an area of about 0.1 deg^2 in the Galactic plane. Unlike the fields studied in the Galactic bulge by Glass et al. (1999) and Omont et al. (1999), this disk field suffers serious interstellar extinction in the Galactic plane. We picked it to make a case study of ISOGAL data in the Galactic disk, taking advantage of the recent availability of the ISOGAL-DENIS PSC. This line of sight is interesting because it crosses four spiral arms, with large values of visible extinction up to 30 mag and beyond, corresponding to strong CO emission (Bronfman et al. 1989). Being much closer to the Galactic Center than the field of the early study by Pérault et al. (1996), at $l = -45^\circ$, it is more typical of the majority of ISOGAL fields. Being outside of the tangential direction of the

Send offprint requests to: B. W. Jiang,
e-mail: bjiang@bnu.edu.cn

⋆ This is paper No. 15 in a journal based on data from the ISOGAL project.

⋆⋆ Based on observations with ISO, an ESA project with instruments funded by ESA Members States (especially the PI countries: France, Germany, The Netherlands and the UK) and with the participation of ISAS and NASA; and on DENIS observations collected at the European Southern Observatory, Chile.

⋆⋆⋆ Table 5 is only available in electronic form at the CDS via anonymous ftp to cdsarc.u-strasbg.fr (130.79.128.5) or via http://cdsweb.u-strasbg.fr/cgi-bin/qcat?J/A+A/400/903

Table 1. Log of observations.

	Filter	Date	ISO ION	pfov
ISOGAL	LW2	1997.03.18	48801636	6″
ISOGAL	LW3	1996.09.26	31500236	6″
DENIS	I, J, K_S	1996.03.25		3″

molecular ring, it avoids too strong perturbations of the quality of ISOGAL data by star forming regions, while keeping nevertheless a non negligible number of detected YSOs. On the other hand, it is far enough from the Galactic Center so that disk sources well prevail against bulge ones, although this direction is neither very far from the far end of the bar structure (e.g. Lopez-Corredoira et al. 2001). In addition to the discussion of stellar populations detected by ISOGAL, which is more difficult than in the bulge because of the larger uncertainty on the distance of the sources, the main goal of this paper is to show how the combination of ISOGAL and DENIS data allows to study the properties and the structure of interstellar extinction in the inner Galactic disk.

2. Observation and data reduction

The observation by the 60-cm space telescope ISO took place towards the center position of $l = -18.63°$ and $b = +0.35°$, i.e. $\alpha = 16^h50^m25.4^s$ and $\delta = -43°58'29''$. The rasters covered a rectangular $l \times b$ area of 0.35×0.29 deg^2. The details of the ISOGAL observation procedure with ISOCAM (Cesarsky et al. 1996) are described in Schuller et al. (2003). The observations of the field FC–01863+00035 were performed with 6″ pixels with the filters LW2 (5.0–8.5 μm, $\lambda_{ref} = 6.75$ μm) and LW3 (12–18 μm, $\lambda_{ref} = 14.3$ μm). The log of ISOGAL and DENIS observations is given in Table 1.

The general processing of the ISOGAL data is described in detail in Schuller et al. (2003). The reduction of the data from the OLP7.0 (OffLine Processing) pipeline was performed by first using the CIA package (Ott et al. 1997). Dark currents are corrected and cosmic-rays are removed. Thereafter, a procedure is applied to simulating the time behavior of the pixels of the ISOCAM detectors, eliminating the related artifacts and improving the photometry. The flat-field and image distortion are corrected. Conversion to magnitudes from the calculated flux density at 7 μm and 15 μm is under the assumption that a Vega model, without circumstellar dust, corresponds to zero magnitude at respective wavelengths, i.e. $[7] = 12.38 - 2.5 \log F_{LW2}$(mJy) and $[15] = 10.79 - 2.5 \log F_{LW3}$(mJy). The current version of the images are shown in Fig. 1. On average, the rms dispersion of the ISOGAL photometry (from repeated observations – see for example Schuller et al. 2003) is estimated to be generally less than 0.2 mag with a small increase for the faintest sources that correspond to about the 50% completeness limit.

In the field FC–01863+00035, the numbers of point sources extracted are 538 and 389 respectively in LW2 and LW3 bands within the limits of magnitude 9.38 in LW2 and 8.16 in LW3, which correspond to the flux limits of about 15 mJy and 11 mJy, respectively (generally such limits are chosen in the ISOGAL PSC such that they correspond to detection completeness ∼50%, Schuller et al. 2003). There are in total 648 ISO sources, out of which 279 objects were detected in both LW2 and LW3 bands, 259 objects detected in only LW2 band and 110 objects detected in only LW3 band. Among the 279 LW2-LW3 associated sources, 257 sources have good association quality flags 3 or 4 and 21 sources have doubtful associations with quality flag 2. We will discard the single association with quality flag 1 hereafter. With the association radius 5.4″, the number of LW2-LW3 spurious associations should be ∼3. The ISO sources are distributed along brightness as shown in Fig. 2. As can be seen from Fig. 2 the detection is certainly not complete to sources fainter than magnitude 9.0 in LW2 or fainter than magnitude 7.5 in LW3. A general tendency is that more brighter sources are detected in both LW2 and LW3 bands while more weaker sources are detected in only one band.

In near-infrared, this ISOGAL field was also observed in the 2MASS survey in the J, H and K_S bands, but the data are not yet available. Contrarily, it was early observed in a special observation of the DENIS survey in the I, J, K_S bands by a 1-m telescope at ESO, La Silla (Simon, in preparation). The DENIS survey has much higher sensitivity (by typically 3 mag in K_S) as well as higher spatial resolution (by about 2−3 times) than the ISOGAL survey. The number of sources detected by DENIS is much larger and limited by confusion in the J and K_S bands. There are 5345, 5817 and 5702 sources in the I, J and K_S bands, respectively. From the distribution of the brightness of these DENIS sources in this field as shown in Fig. 3, the detections in the near IR bands are reasonably complete to I = 16 mag, J = 14 mag and K_S = 12 mag.

In order to keep the population of spurious DENIS-ISOGAL cross-identifications below a few percents, the association was limited to K_S-detected sources with $K_S < 12.9$ (shown by a long-dash line in the right panel of Fig. 3), corresponding to a density of K_S sources $n = 36\,000$/deg^2. Such a density limit is systematically applied in the ISOGAL PSC for the DENIS association radius. It is chosen such as $n\pi r_a^2 = 0.1$, where $r_a = 3.5''$ is the main association radius. The numbers of sources associated with a DENIS source in the ISOGAL PSC are thus 479 objects in the LW2 band and 270 objects in the LW3 band. Among these objects, 16 LW2 sources and 18 LW3 sources (in total 24 sources only) are poorly associated with the DENIS objects, i.e. their association quality factors are either 1 or 2 in the ISOGAL PSC (see for details from Schuller et al. 2003) and they are dropped for later discussion. The numbers of associations with quality flag equal to 3 are 9 in the LW2 band and 10 in the LW3 band (15 sources in total); they mainly correspond to association radius between r_a and $2r_a$. The associations with quality factors 4 or 5 (463 sources) are very probably real associations with a proportion of spurious associations less than ∼2%. The associations with quality flag 3 still have a good chance to be real, but with a larger proportion of spurious associations; in this field however no such objects have association radius larger than 5″. Among the 538 LW2 objects, 463 (86% of all LW2 sources) are thus reasonably well associated with the DENIS K_S sources, 351 are also detected in the J-band and 109 in all DENIS bands. Among the 389 LW3 objects, 252 (65% of all LW3 sources) are reasonably well

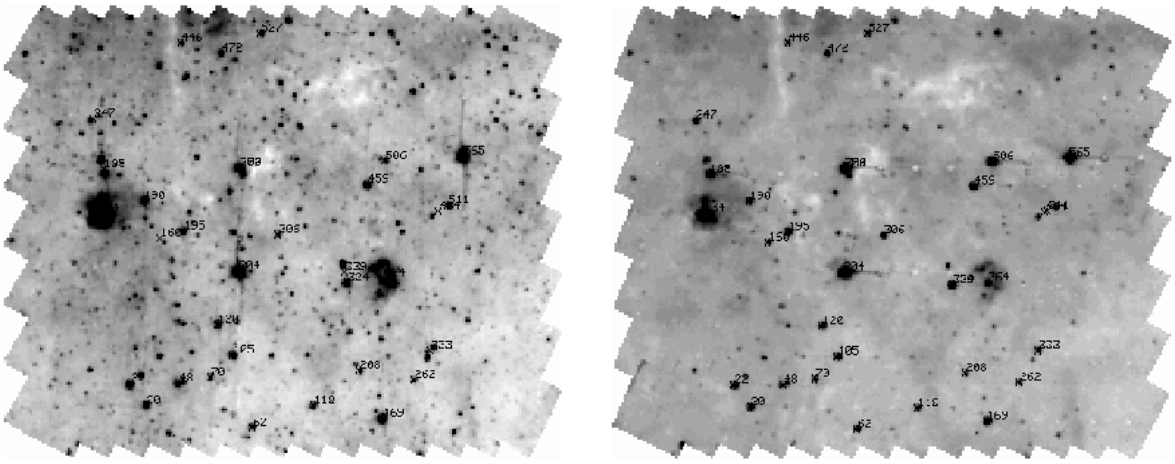

Fig. 1. The ISOCAM images of the field FC–01863+00035 in LW2 (left) and LW3 (right) bands. Increasing l is to the right and increasing b is downwards. The sources with [7] < 5.0 or [15] < 5.0 are labeled by the sequence numbers in the ISOGAL PSC catalog. (See Table 4 for those detected by IRAS.)

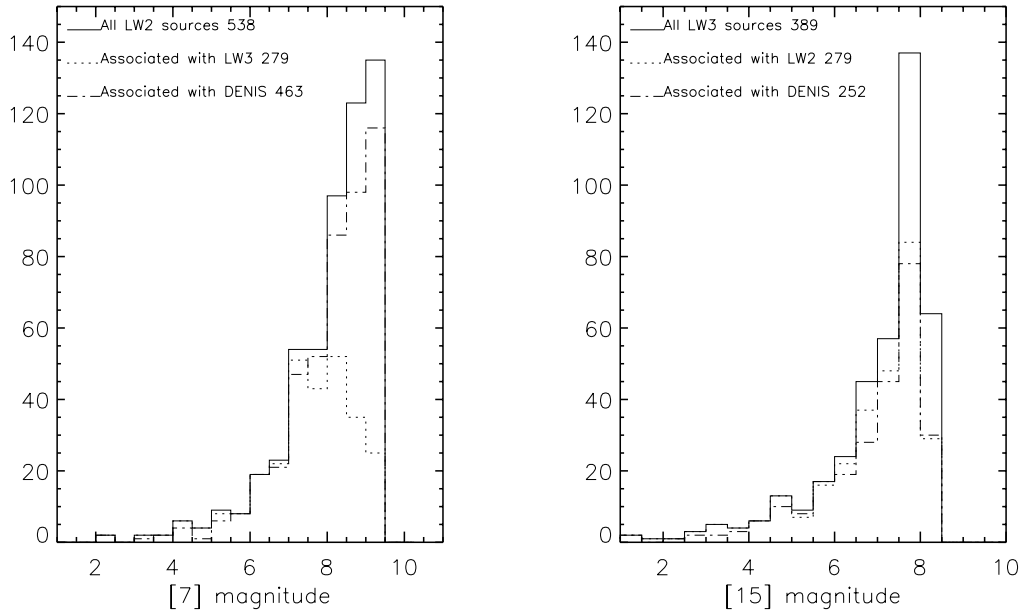

Fig. 2. The sources detected in the ISOGAL observation. The solid line histogram shows the distribution of all ISOGAL sources, the short dash line shows the distribution of the sources associated with the other ISOGAL band and the dash-dot line shows the distribution of the sources detected during the DENIS survey where only the sources with good association flags are counted. The left graph is the histogram of LW2 sources and the right one is of LW3 sources.

associated with the DENIS K_S sources, 198 are also detected in the J-band and 54 in all DENIS bands. Three DENIS sources associated with ISOGAL have a bad quality in K_S because of saturation ($K_S < 6.5$), and one J-associated source is saturated ($J < 8.0$). One can check on the DENIS K_S and J images that five strong sources present at the position of strong ISOGAL sources are missing in the DENIS catalog because of saturation (Sect. 4.3). From Fig. 3 it can be seen that most of the DENIS objects with $K_S < 9$ with 11 exceptions were detected by ISO. Among the ISOGAL sources that are not associated with the DENIS sources, 31 are detected in both LW2 and LW3 bands, 27 in only LW2 band and 87 in only LW3 band. There are 15 LW3 objects associated with K_S objects and with association quality flag ≥3, but are not associated with LW2 sources. They may be spurious cross-identification between DENIS and ISOGAL catalogues and are dropped in the following discussions.

The details of the results including the astrometric, photometric and association information of all the ISOGAL objects will be available on the web in the ISOGAL-DENIS PSC via `http://vizier.u-strasbg.fr/viz-bin/VizieR` and `http://www-isogal.iap.fr` (Schuller et al. 2003).

3. Interstellar extinction

This field FC–01863+00035 at $b = 0.35°$ is close to the Galactic mid-plane where the interstellar extinction is serious. The measurement of interstellar extinction becomes then

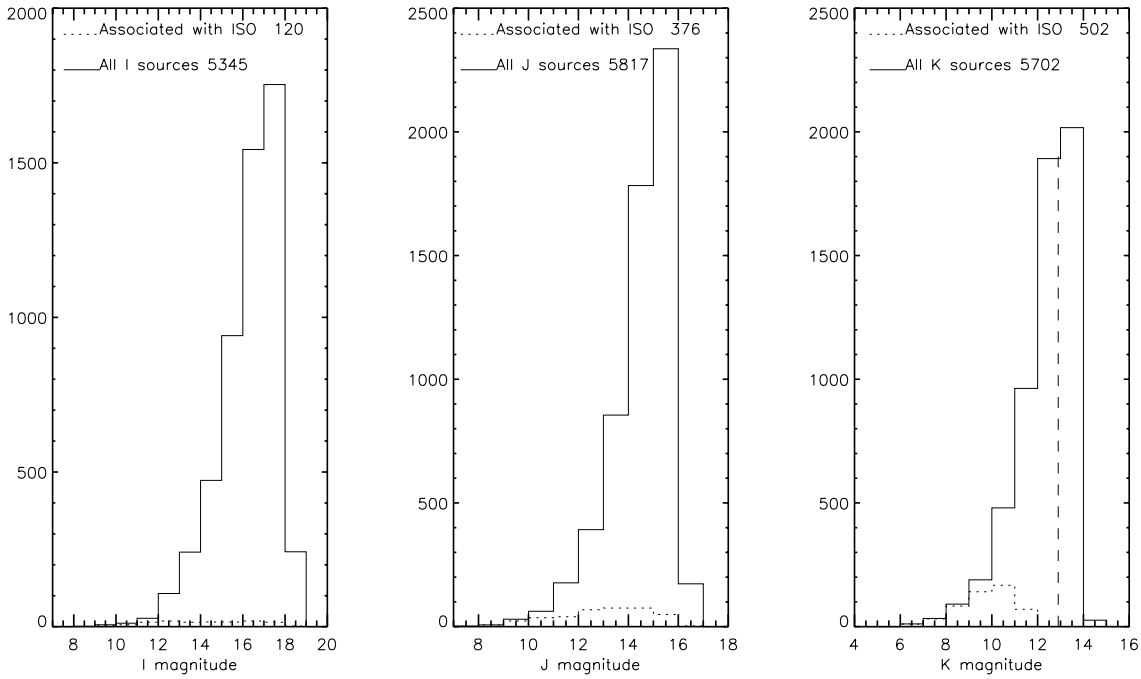

Fig. 3. The DENIS sources in the ISOGAL field. All the sources detected by DENIS in the same field are distributed as indicated by the solid line. Those associated with the ISOGAL objects are represented by the short-dashed line and their number are also shown in the upper part of the graphs. From left to right are aligned bands I, J and K_S. In the graph of the K_S-band, a long-dashed vertical line marks the limit $K_S = 12.9$ mag used for searching DENIS association.

impossible in optical at large distances. Based on the optical observations of O-type to F-type stars, the A_V value at the direction of $l = -18°$ and $b = -0.5°$ which is close to the ISOGAL field, is estimated to be about 3 mag and approximately constant from a distance of ∼1 kpc up to ∼4 kpc (Neckel & Klare 1980). This may be a good reference for short distances although the patchy distribution of interstellar matter in the Galactic plane (Schultheis et al. 1999) may lead to some significant difference from the extinction in the ISOGAL field FC–01863+00035. However, the sources detected in the mid-infrared LW2 and LW3 bands extend to a much larger distance because of the much smaller extinction at these wavelengths than in optical.

Our calculation of interstellar extinction is based on two assumptions. One is that most of the objects in the ISOGAL field are luminous RGB stars or AGB stars with moderate mass loss rate. These objects are very bright with a luminosity of about one thousand to several thousand solar luminosity, and cold with an effective temperature lower than 4000 K or so. In addition, stellar winds from the photosphere have formed a circumstellar envelope for many of them. So they are strong emitters in mid-infrared. The analysis of the ISOGAL fields at ($l = 0.0°$, $b = 1.0°$) and in Baade's Window, has actually found most of the sources there are RGB and AGB stars whose colors are mildly reddened by interstellar extinction (Omont et al. 1999; Glass et al. 1999). The other assumption is that the intrinsic colors $(J-K_S)_0$ of all these sources are approximately similar as well as $(K_S–[7])_0$, which is not true for the minority of objects with large mass-loss. According to the compilation of Wainscoat et al. (1992), the value of $(J-K)_0$ of an M 0III star is about 1.0 and of an M 5 early AGB star is about 1.3 (see also van Loon et al. 2003 and references therein). In one ISOGAL field Sgr I that is inside the Baade's Window (Glass et al. 1999), the concentration of $(J-K_S)_0$ and $(K_S–[7])_0$ is very evident; for the objects with $(K_S–[7]) < 1.0$, the average $(J-K_S)_0$ is 1.08 with standard deviation of 0.17 mag and the average $(K_S–[7])_0$ being 0.20 with standard deviation of 0.23 mag (with the revised photometry of the ISOGAL PSC, see Sect. 3.1) when the interstellar extinction is subtracted as 0.2 mag in the K_S-band.

3.1. Extinction law at 7 and 15 micron

The assumption to start to extract the extinction law in mid-infrared is that the intrinsic color index $(J-K_S)_0$ of most stars in the field is the same so that their observed color $J-K_S$ represents the interstellar extinction. Another presumption is the linear correlation between two color indexes if they are both originated from interstellar extinction, e.g. a linear correlation between the interstellar reddening at $J-K_S$ and K_S–[7], and at $J-K_S$ and K_S–[15]. For the first assumption, we had to remove some objects with apparently different intrinsic color. In addition to RGB stars and AGB stars with moderate mass loss, YSOs and AGB stars with high mass loss may be important members of the mid-infrared objects. Their cold and thick circumstellar envelopes absorb near-infrared radiation and radiate in mid-infrared strongly and make them easily detected by the ISOGAL survey. Their intrinsic color indexes $(K_S–[15])_0$ and $(K_S–[7])_0$ [and even $(J-K_S)_0$ for some of them] are redder than RGB stars or early AGB stars, and their color index [7]–[15] is also redder. Because the observed values of $J-K_S$, K_S–[7] and K_S–[15] are significantly influenced by interstellar extinction, they can not be used as a criterion to pick up the late AGB stars or YSOs. On the other hand, the interstellar extinction in the LW2 and LW3 bands is much smaller, the color

index [7]–[15] should be affected little by interstellar extinction. From the ISOGAL results in the Baade's Window (Glass et al. 1999) and from modeling (Ojha et al. 2003) we estimate that, for [7]–[15] < 0.4, the effect of circumstellar dust of AGB stars is negligible on $(K_S–[7])_0$, that it remains small ($\lesssim$0.3) on $(K_S–[15])_0$, and that it is similarly negligible on $(J–K_S)_0$ for [7]–[15]<1.0. Therefore we exclude the stars with [7]−[15] > 0.4 or [7] − [15] > 1.0 in the discussion of the relation of the colors K_S–[7] and $J–K_S$, respectively, with interstellar extinction. Applying the same criteria for young stars also warrants that the effect of circumstellar dust is negligible on their intrinsic colors (see e.g. Bontemps et al. 2001).

If we set the intrinsic color $(J–K_S)_0$ of most ISOGAL stars as $C^0_{JK_S}$ and of $(K_S–[7])_0$ as $C^0_{K_S7}$, and the observed color indexes as $C_{JK_S} = J–K_S$ and $C_{K_S7} = K_S–[7]$ accordingly, the linear relationship is expected to be $C_{K_S7} - C^0_{K_S7} = k\ (C_{JK_S}– C^0_{JK_S})$. Based on model calculation (e.g. Bertelli et al. 1994) and the observation of the field Sgr I, the intrinsic color $C^0_{JK_S}$ of RGB stars or early AGB stars is taken to be 1.2 on average, while the intrinsic color index $C^0_{K_S7}$ of these stars is not well known (however, see van Loon et al. 2003). By leaving $C^0_{K_S7}$ as a variable and assuming that the observed C_{K_S7} of sources with [7]–[15] < 0.4 is mainly caused by interstellar extinction, a robust linear fitting method, which minimizes absolute deviation and is insensitive to large departures for a small number of points, was used to fit the data and the result is displayed in the color-color diagram (Fig. 4, left). The resulted values for this linear fitting to the points decoded by pluses and triangles in Fig. 4 are: $k = 0.35$ and $C^0_{K_S7} = 0.34$ (assuming $C^0_{JK_S} = 1.2$).

The processing of K_S–[15] is similar to that of K_S–[7]. The results are then $k = 0.39$ and $C^0_{K_S15} = 0.39$ (assuming $C^0_{JK_S} = 1.2$) (Fig. 4, right). In Fig. 4, the sources with [7]–[15] > 0.4 are displayed by diamonds though they were abandoned during the fitting process to both the K_S–[7] and K_S–[15] with $J–K_S$. Their large deviation to the right side from the fit line further proves that they are intrinsically redder. However, there could be a residual effect of circumstellar dust on the value of K_S–[15] even for sources with [7]–[15] < 0.4, especially for sources with large values of $J–K_S$ which are more luminous; it could lead to an overestimation of k by maybe ∼10–20%.

For a blackbody radiation at temperature 4000 K typical of an M 0 RGB star, the Planck function yields $C^0_{K_S7} = 0.35$ and $C^0_{K_S15} = 0.44$ when the flux density for $K_S = 0.0$ is taken as 6.65×10^{24} W/m^2/Hz (Schuller et al. 2003), which is consistent with the fitting results $C^0_{K_S7} = 0.34$ and $C^0_{K_S15} = 0.39$. Our values of $C^0_{K_S7}$ and $C^0_{K_S15}$ are in reasonable agreement with those from Glass et al. (1999) in Baade's Windows when one takes into account the correction of −0.45 mag to be applied to the preliminary ISOGAL photometry used by Glass et al. (1999) (Schuller et al. 2003).

The linear coefficients between C_{JK_S} and C_{K_S7} or C_{K_S15} define the extinction values at 7 and 15 microns which depend on the extinction values in near infrared. With the extinction values in near infrared given by van de Hulst (1946), Glass (1999) and Rieke & Lebofsky (1989), the corresponding values at 7 and 15 microns are calculated and listed in Table 2 by adopting the coefficients $k = 0.35$ and $k = 0.39$ between C_{JK_S} and C_{K_S7}, and C_{JK_S} and C_{K_S15}, respectively.

While the extinction values in the near-infrared from Rieke & Lebofsky (1989) are higher, the ones preferred by Glass (1999) are just an update of those of van de Hulst (1946) and thus the two latter sets of values are quite close to each other. Similarly, the extinction values at 7 and 15 μm derived from Rieke & Lebofsky ($A_7 \approx A_{15} \approx 0.05$) are higher than those inferred from Glass–van de Hulst, i.e. $A_7 \approx 0.03A_V$ and $A_{15} \approx 0.025\mathrm{A}_V$ (see Table 2). As generally in other ISOGAL papers, we prefer Glass' values for the reasons exposed in Glass (1999), except possibly for the fields close to the Galactic Center and in star forming regions. To compare the values we have derived for the mid-infrared extinction with previous ones, we will distinguish the case of 7 μm where the fitting of Fig. 4 (left) is very robust, from the one of 15 μm which is more uncertain. In both cases one should note that the averages of the extinction on the wavelength range of the LW2 and LW3 broad bands yield slightly larger values than at 7 and 15 μm, respectively, which are both close to a minimum of the extinction curve.

At 7 μm the most widely used reference for the extinction value is probably Mathis (1990) which is similar to Draine & Lee (1984). They used similar extinction law in near infrared to Rieke & Lebofsky (1989), and estimated the infrared extinction from an extrapolation of the optical extinction law and near-infrared observational data, yielding $A_7 \sim 0.020\ A_V$. This value is slightly lower than the one we derived, $0.03\ A_V$. Such a difference may arise from the uncertainty in the ISOGAL photometry or in the fitting procedure in Fig. 4. It is probably included as well within the uncertainty of the extrapolation by Mathis (1990). We will use our value, $0.03\ A_V$, in the following of this paper, keeping in view its uncertainty. Let however note that the higher value we could derive from the near-infrared extinction law of Rieke & Lebofsky (1989) (Table 2), is also consistent with the results derived by Lutz (1999) ($A_7 \approx 0.045$) who used the hydrogen recombination lines and the same near-infrared extinction law towards the Galactic Center.

The extinction ratio A_7/A_{15} is given as ∼1.3 by Mathis (1990). However, the value of Draine & Lee (1984) is almost twice smaller. The best value for this ratio has probably been derived by Hennebelle et al. (2001) from an analysis of infrared dark clouds from the ISOGAL survey. They give 0.7 ± 0.1 for the clouds away from the Galactic Center, which is similar to Draine & Lee (1984). The value we derived for this ratio in Table 2, Col. 2, 1.2, is more compatible with Mathis (1990) than with Hennebelle et al. (2001). In Fig. 4 (right), the 15 μm value deduced from the Hennebelle et al. ratio is shown by a dashed line derived from the extinction values at J, K_S and 7 μm taken from Col. 2 of Table 2. It is evident that their result implies more extinction at 15 μm. However, let us stress that our direct fitting is somewhat uncertain at 15 μm because of the smaller number of sources and of the possibility of residual effects of circumstellar reddening on K_S–[15], especially for the distant luminous sources with large extinction. Therefore, we consider that the 15 μm value deduced from Hennebelle et al. (2001) (dashed line in Fig. 4 (right)) is still compatible with the data of our fitting in Fig. 4 (right, full line), and that our

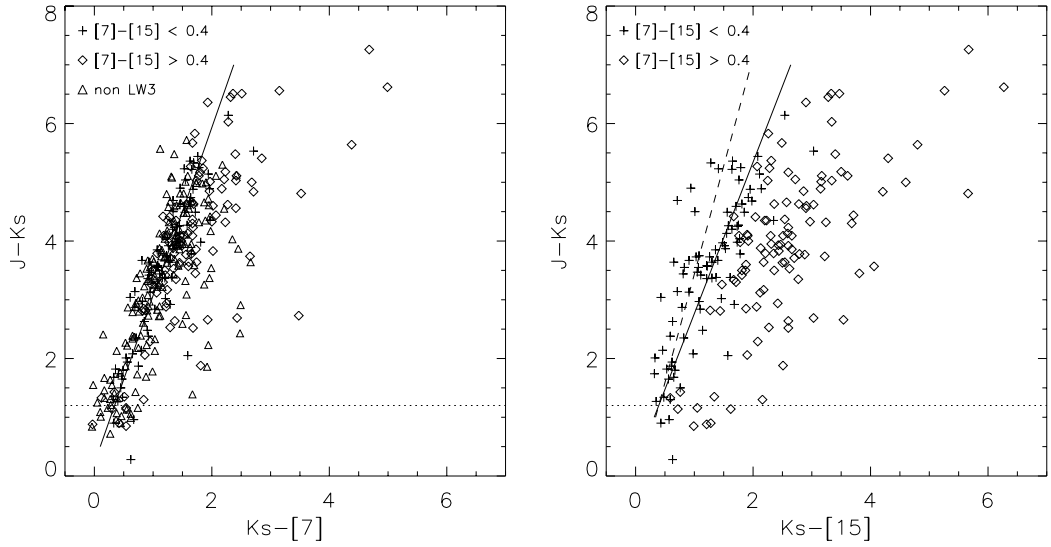

Fig. 4. Color-color diagram of $J-K_S$ vs. K_S–[7] and $J-K_S$ vs. K_S–[15]. The sources detected in the LW3 band are divided into two groups, one with [7]−[15] < 0.4 decoded by pluses which were used for linear fitting and the other with [7]−[15] > 0.4 decoded by diamonds which were not used for linear fitting. In the left graph, the sources which are not detected in the LW3 band but are used in linear fitting are decoded by triangles. The robust linear fitting result is shown by solid line. The horizontal dot line labels where $J-K_S = 1.2$ which is assumed intrinsic color $J-K_S$ for the sources used in fitting. In the right graph, a dash line represents the result of combining the 7 to 15 μm opacity ratio from Hennebelle et al. (2001) with the extinction values of J, K_S and 7 μm in Col. 2 of Table 2 (i.e. $A_{15} = 0.044$).

Table 2. Extinction values in the LW2 (7 μm) and LW3 (15 μm) bands.

Band	A_λ/A_v		
	vdH[1]	ISG[2]	R & L[3]
J	0.245	0.256	0.281
K_S	0.087	0.089	0.112
7	0.032	0.031	0.053[4]
15	0.026	0.025	0.046

[1] Values for J and K_S derived from van de Hulst (1946) curve.
[2] Values for J and K_S derived from Glass (1999) (update of van de Hulst's values).
[3] Values for J and K_S derived by Rieke & Lebofsky (1989) for stars towards the Galactic center.
[4] 7 and 15 μm extinction values are then derived from the slopes k of the straight lines of Fig. 4 (see text): $A_{K_S}-A_7 = 0.35(A_J-A_{K_S})$, $A_{K_S}-A_{15} = 0.39(A_J-A_{K_S})$.

data cannot provide a really accurate value of the extinction at 15 μm. Nevertheless, we will use the values derived from our fitting in the subsequent sections, since such differences on the small extinction at 15 μm are practically negligible in the following discussions. One has to keep in mind that the extinction law may vary with the directions due to the inhomogeneous distribution of the interstellar matter in the Galactic plane.

3.2. Extinction structure along the line of sight

By assuming the intrinsic color index $C^0_{JK_S}$ is the same for all the objects which were detected in both J and K_S bands and with [7]−[15] < 1.0 if detected in both LW2 and LW3 bands as well, the interstellar extinction to individual objects can then be calculated from the observed C_{JK_S}. Theoretical calculation shows that $C^0_{JK_S}$ doesn't differ much for late-type RGB stars and early AGB stars which are the major components of the ISOGAL sources. Though there may be some foreground main-sequence stars and early-type AGB stars with intrinsic bluer color than late-type RGB stars that would bring about the underestimation of A_V, the number of such sources should be small and they should be mostly at small distance to be detectable by ISOGAL as seen in Fig. 4 for those with $J-K_S < 1.0$. While many of the ISOGAL sources are detected in the K_S-band and not detected in the J-band, the value of A_V may then be inferred from C_{K_S7} according to the extinction law derived above. This method is right only if the non-detection in the J-band is caused by large interstellar extinction. Because some of the non-detections in the J-band may come from serious absorption by circumstellar dust of AGB stars or YSOs, the estimation from C_{K_S7} may overestimate the real interstellar extinction, in particular when the index C_{K_S7} is large, e.g. larger than 2 that results in $A_V \sim 30$. So when inferring the extinction value from K_S–[7], we have excluded the sources with [7]−[15] > 0.4 because of the risk they present the occurrence of large mass loss. For the same reason, we have excluded the sources with [7]−[15] > 1.0 when inferring the extinction value from $J-K_S$. However, we have thus altogether discarded a large proportion of sources with the largest extinction.

We adopted the value of intrinsic color index $C^0_{JK_S}$ as 1.2 and the extinction values listed in Col. 2 of Table 2. The global distribution of A_V is shown in Fig. 5d, where values of A_V from $J-K_S$ or K_S–[7] are distinguished by the dash or dot lines respectively, while the summation of the two types is represented by the solid line. It can be seen, as expected, that the sources not detected in the J-band experience higher extinction than those detected in the J-band on average. All the sources not detected in the J-band have $A_V > 10$ and peak at about 28. In Fig. 5, we have added to the bin $A_V = 0$–2 all the sources with $J-K_S < 1.2$. Such sources should not be AGB or RGB-tip

stars, but nearby earlier stars, mostly K giants with a few A-B stars. Most of them must have $A_V < 2-3$. We have checked that the corresponding values of I–J are consistent with J–K for all these 19 sources, except for one where there is a problem with the DENIS I–J associations. As expected, all of them are associated with a visible GSC2–2 star. The combined visible/near-infrared colors are consistent with K-early or M giants for most of them, with, however, an identified A2 star.

In addition to the concentration at $A_V \sim 0$, the sources are distributed along A_V unevenly. After a dip at $A_V \approx 4-6$, there is first a progressive increase of their number up to $A_V \approx 12$, and then a steeper rise until a relatively sharp maximum at $A_V \sim 14-16$. After that, their number decreases rather regularly up to $A_V \sim 50$.

We think that the uneven distribution of A_V reflects the inhomogeneities in the distribution of the interstellar medium, partly along the line of sight with the crossing of the molecular ring and of several arms, but probably mainly perpendicular to the line of sight across the observed ISOGAL field. In order to see the influence of the spiral arms, we estimated the extinction values to the arms from the distribution of the emission in the radio lines of CO and HI. The kinematical distance to the interstellar clouds can be inferred from their radial velocity. The line of sight in the direction $l = -18.63^\circ$ and $b = 0.35^\circ$ touches the outer edges of the Sagittarius, the Centaurus and the Norma arm at respectively 1, 4, and 6 kpc, runs through the bulge and then reaches the far side of the Norma arm at about 13 kpc. Indeed, most of the line of sight, between 3 to 13 kpc, is in the molecular ring, including the tangential point at ~8 kpc ($v \sim -130$ km s^{-1}).

As for the whole Galactic disk, there exist ^{12}CO data for our field taken from the Milky Way survey at the coarse resolution of 0.125° (7.5′) (Dame et al. 2001). Our $0.35^\circ \times 0.29^\circ$ field thus implies nine pointings of this survey at $l = 18.625^\circ \pm 0.125^\circ$ and $b = 0.375^\circ \pm 0.125^\circ$. A rapid look at these CO emission data shows that it corresponds mainly to radial velocities characteristic of the molecular rings and more precisely, of the Centaurus and Norma arms. However, there is an ambiguity for the emission between -70–-80 km s^{-1} which could be attributed either to the near side or to the far side of Norma. Especially in the Centaurus arm, the CO emission displays a strong gradient with respect to b across this field (Table 3). In order to take into account this gradient in the discussion of the distribution of A_V, we will consider separately the three b ranges of the pointings of the CO survey (Table 3). For each b range of the pointings we computed the CO integrated intensity, W_{CO}, averaged over the three l pointings, for each velocity interval roughly corresponding to the different spiral arms (Table 3). Then we estimated the corresponding A_V shown in Table 3, adding a contribution from the HI regions from the HI survey of Bloemen et al. (1990).

We estimated A_V shown in Table 3 by adopting the conversion factor 1.8×10^{20} cm^{-2} (K km s^{-1})$^{-1}$ from the CO integrated line intensity W_{CO} to H_2 column density (Dame et al. 2001) and the factor 10^{21} molecules cm^{-2} mag^{-1} from H_2 column density to A_V. This estimation, in particular of the HI column density, suffers some uncertainty from integrating the velocity on unclear contours of the paper that could be about 30%. The W_{CO} to N_{H2} conversion factor is also known to be rather uncertain (Bachiller & Cernicharo 1986; Harjunpaa & Mattila 1996).

Similarly, we split our sample of ISOGAL sources in three unequal parts corresponding to these b ranges (Table 3). For each subsample, we have represented in Fig. 5 the histogram of the distribution of A_V. We note, as expected, important differences in the total ranges of these three distributions reflecting the gradient of the extinction with b.

In view of discussing the correspondence between the A_V distribution from the ISOGAL sources and the determination from the interstellar gas, let us stress the difficulty that any spatial inhomogeneity in the CO intensity smaller than the large CO beam is smoothed with the present CO data. Therefore, it is impossible to estimate the actual spatial dispersion of A_V within a spiral arm. It is certainly significantly larger than the dispersion, ~20%, between the three l pointings for the same b range. In each of the three histograms of Fig. 5 the average value of the accumulated extinction expected from the interstellar gas just beyond the Centaurus arm is, $A_{Vc} = 23$, 18 and 12, respectively (Table 3). Looking at the values of the sharp rise of the A_V distribution due the Centaurus arm, with $A_{Vc1} = 12$, 14 and 10, respectively, one sees that these are 20-50% lower than A_{Vc}. A natural interpretation is that this difference essentially represents the dispersion of the extinction through the Centaurus arm. The case of the subfield with $b > 0.4375^\circ$ is special because the b sample observed by ISOGAL, $0.4375^\circ < b < 0.495^\circ$ is about half the total range of the CO pointing, $0.4375^\circ < b < 0.5625^\circ$. Because of the strong gradient with b, it is likely that the average extinction in the region observed by ISOGAL is larger than the one in the total CO beam which yields $A_{Vc} = 12$ (see Table 3). Indeed the main feature of Fig. 5c is approximately symmetric with respect to $A_{Vc'} = 14$, which should be close to the actual value of the average of A_V in the region observed by ISOGAL. However, it is unclear in this case whether the main contribution of Norma is absent because it comes from the far side with very few sources behind it, or it is included in the pedestal between $A_V = 18$ and $A_V = 22$, together with the extinction of a few sources behind the tangential point region.

The situation is less clear for the other two subsamples with smaller b and larger extinction. It is true that the distribution again extends beyond the value A_{Vc2}, symmetric of A_{Vc1}, with respect to A_{Vc}, as expected from such a dispersion of the A_V distribution through the Centaurus clouds and the additional extinction beyond Centaurus. But there is a large decline of the number of the sources towards large A_V, making the distribution very asymmetric with respect to A_{Vc}. The loss of sources may be explained by the very large value of A_V which prevents the detection at 7 μm or even in the K_S-band of many sources.

Finally, we note that for the three subsamples, the total range of values of A_V inferred from the ISOGAL sources is consistent with the maximum accumulated extinction along the line of sight expected from the interstellar gas, including the dispersion of A_V values within clouds, the Norma ambiguity and the loss of sources with very large A_V.

Despite the many uncertainties in the relation between W_{CO} and the ISOGAL colours and in the interpretation of the A_V distribution, one feature remains intriguing. Before the sharp rise

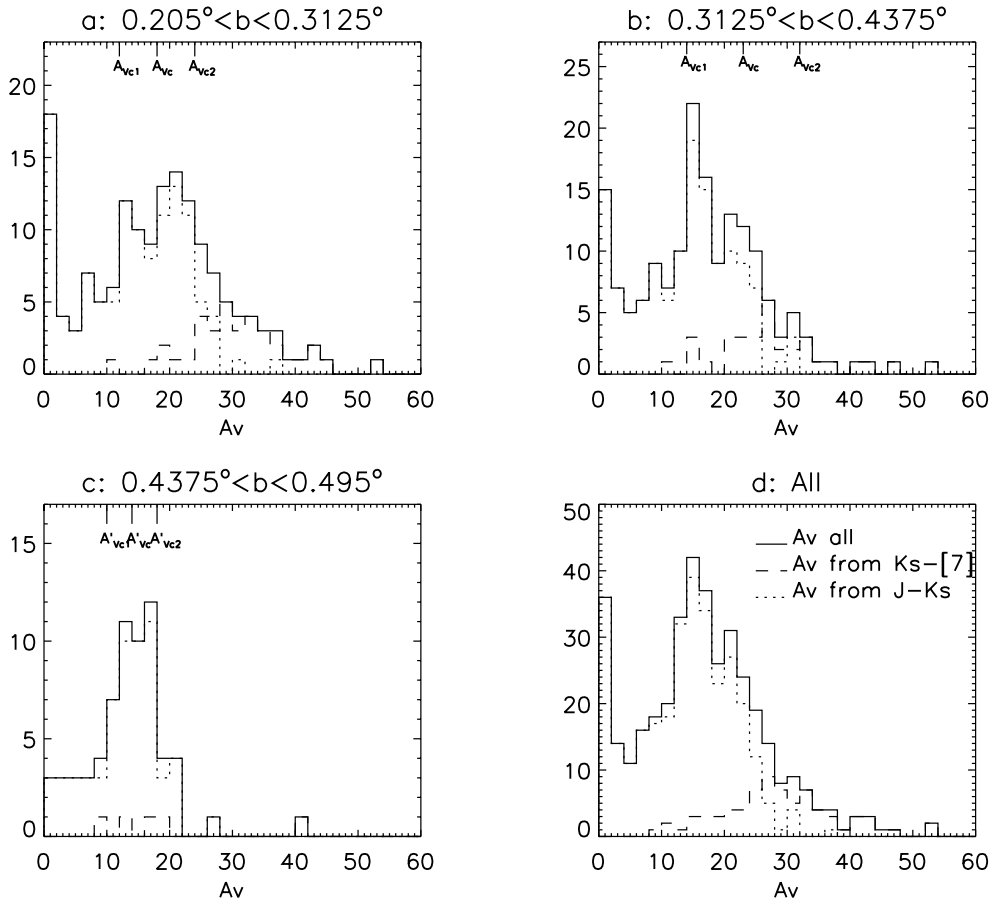

Fig. 5. Histograms of the interstellar extinction A_V, which are derived either from $J-K_S$ (dot line) or from K_S–[7] (dash line) when no data in the J-band are available (sources with [7]–[15] > 0.4 are excluded), and from the addition of these two types (solid line). Figures **a)**, **b)** and **c)** display the sources with b in the quoted ranges corresponding to the overlap of the ISOGAL field with the pointings of the CO survey data by Dame et al. (2001). Figure **d)** shows the extinction distribution of the sources spanning the whole b range in this field. A_{Vc} represents the average value of the accumulated extinction expected from the interstellar gas just beyond the Centaurus arm (last line of Table 3); A_{Vc1} represents the starting value of the extinction by the Centaurus arm as deduced from the sharp rise of the A_V histogram; and A_{Vc2} is the symmetric value of A_{Vc1} with respect to A_{Vc}, which could correspond to the ending value of the extinction by the arm. The same method cannot be applied to subfield "c" because the ISOGAL range is about half, much smaller than the total range of the CO pointing; $A_{Vc'}$ is instead defined as the average value of the peak of the histogram.

at $A_V \sim 10$–14 that we associate with the Centaurus arm, there is a distribution of a smaller number of sources from $A_V \sim 6$ to ∼12. The local and Sagittarius arm emission of CO is quite unable to account for such extinctions. The only explanation is that such sources are located within the Centaurus arm, behind the first dust layers. The subsequent very sharp rise suggests a narrow distribution of the bulk of the Centaurus extinction. The appreciable number of sources with $A_V \sim 6$ to ∼12 suggests that the first Centaurus layers of dust are distributed over a rather large distance with a substantial source density. This implies a large width for the Centaurus "arm", which is consistent with the broad CO velocity distribution, and/or an overdensity of ISOGAL sources inside it, which could be mostly young/massive K giants.

4. Stellar populations

4.1. Sources detected in the J-band

For the ISOGAL sources which are detected in both J and K_S bands during the DENIS observation a correction for interstellar extinction can be applied to observed color indexes such as K_S–[7], K_S–[15] and [7]–[15]. The group of extinction values we used are in Col. 2 of Table 2. The color magnitude diagrams $(K_S-[7])_0/[7]_0$ and $(K_S-[15])_0/[15]_0$, are shown in Figs. 7 and 8 for the sources detected in both J and K_S bands. They are compared with the diagrams of the ISOGAL sources in the Baade's Window Sgr I where the interstellar extinction is much smaller. Specifically, the extinction in the K_S-band in the Sgr I field is taken to be 0.2 mag and no extinction is taken into account there for the LW2 and LW3 bands (Glass et al. 1999). In the color-magnitude diagram [7]–[15]/[15] of our field FC–01863+00035 (see Fig. 6), we have not applied the correction for interstellar extinction because it is relatively small in both [7]–[15] and [15] (especially in [7]–[15]), and not certain for both.

In these color-magnitude diagrams, the distribution of most of the ISOGAL objects of the field FC–01863+00035 detected in the J-band is very similar to that of Sgr I, with some small differences. The cluster of stars at the tip of RGB which is seen in the Sgr I field around [7]–[15] = C_{715} = 0.2, [15] = 8.0 or

Table 3. Average interstellar extinction A_V in different distance and b ranges (inferred from Dame et al. 2001 and Bloemen et al. 1990).

	Nearby			"Centaurus"			"Norma"			"Tangent point"		
Distance(kpc)	0–3			3–6 or 7–11			6–8			7–10		
V_{LSR}(km s^{-1})	>0			[0, −60]			[−60, −100]			[−110, −150]		
b[1]	a	b	c	a	b	c	a	b	c	a	b	c
A_V(H_2 via CO)	1.3	0.6	0.6	16.6	13.5	8.5	5.2	6.6	3.1	5.6	3.3	1.4
A_V(HI)/A_{CO}	1			0.25			0.60			0.70		
Accumulated extinction												
Distance(kpc)	0–3			0–6			0–7[2]			0–10		
A_V(H_2+HI)	2.5	1.2	1.2	23.3	18.1	11.8	31.7	28.8	16.8	41.2	34.3	19.0

[1] The range of b of the three CO subsamples are: a: 0.1875° < b <0.3125°, b :0.3125° < b <0.4375°, c: 0.4375° < b <0.5625°.
[2] Assuming that the CO emission is due to the near side of the Norma arm; otherwise, the 6–7 kpc extinction should be much smaller.

$(K_S–[15])_0 = C^0_{K_S15} = 0.3, [15]_0 = 8.0$, does not appear clearly among the LW3 sources in the disk field FC–01863+00035. Instead there is a loose branch of stars along the line $C_{715} = 0.2$ or $C^0_{K_S15} = 0.3$ with width of about ±0.2 magnitude which are probably also RGB stars. Because the sources in the disk field FC–01863+00035 span a wider range of distance than the concentration mostly in the bulge in the case of the Baade's Window, their apparent luminosity in bands LW2 and LW3 scatters more. The intermediate AGB stars, which are fainter by one or two magnitudes in absolute K_S or M_{bol} and lose mass at lower rate than very luminous AGB stars (Omont et al. 1999), appear in the region next to RGB branch with a redder color C^0_{715}. The stripe from $C_{715} = 0.5, [15] = 7.5$ to $C_{715} = 1.0, [15] = 6.0$ coincides well with the location of intermediate AGB stars in Sgr I. Upper along this sequence are the luminous AGB stars with redder color, approximately in the same region as Mira variables in the Sgr I field (Glass et al. 1999). Several stars are brighter than magnitude 4 at [15], which is lacking in the Sgr I field. These stars are mostly identified in the IRAS PSC catalogue due to their strong flux density at 12 μm. They are discussed in a separate subsection. Many of them are clearly much closer than the bulge distance and illustrate the fact that the AGB sequence is not as well defined as in bulge fields because of the wider spread in distances.

4.2. Sources not detected in the J-band

Non-detection in the J-band by DENIS can be due to three reasons. The most frequent one is that interstellar extinction absorbs most of the stellar radiation in the J-band. The second is that the J absorption is due to a very thick and cold circumstellar envelope. Finally a few very strong J sources may not figure in the DENIS catalogue because they are badly saturated (Sect. 2). The reddest color indexes $J−K_S$ of objects detected by ISOGAL and DENIS J and K_S in this field go up to about 7, corresponding to $A_V = 35$ mag if $(J−K_S)_0 < 1.5$. The J detections are relatively complete only to $J−K_S = 5$, i.e. $A_V \sim 25$, which approximately corresponds to the cumulated average extinction of the Centaurus and Norma arms (Sect. 3.2). The non detections in the J-band are mainly due to a very large extinction which may arise either because the star is behind a concentration of interstellar matter in the Centaurus (or Norma) arm, or because it lies much farther in the molecular ring. Their observed color K_S–[7] is on average about one magnitude redder than those detected in the J-band. This tendency can be seen from the color-magnitude diagram of Fig. 7. If the rough relationship derived from the objects detected in the J-band between K_S–[7] and $J−K_S$ is applicable to the non-detections in the J-band, then one magnitude difference in K_S–[7] corresponds to 3 mag difference in $J−K_S$, i.e. about 18 mag difference in A_V.

There are some J-nondetections whose location in the color-magnitude diagram can not be explained by interstellar extinction alone. They are bright in the LW2 or LW3 band, e.g. [7] < 7.0 and [15] < 6.0. Their color index [7]–[15] is around 1.0 that indicates much circumstellar matter. They are good candidates for luminous Mira variable. These stars are at the center of Fig. 6, right-upper of Fig. 7.

Several J-nondetections are not so bright as the candidates for Miras. They are on the contrary a little faint in the LW3 band, from about [15] = 7.0 to [15] = 8.5. Their color index [7]–[15] is usually redder than 1.0. These could be YSOs judged from the relatively low luminosity and excess emission in the LW3 band. In Fig. 6 they are in the middle-lower corner and a similar position in Fig. 8.

4.3. Sources not associated with DENIS

The sources which are not associated with DENIS can be divided into three groups according to the ISO bands of detection: in both LW2 and LW3 bands, only LW2 band and only LW3 band.

The sources detected in both LW2 and LW3 bands, but not in DENIS, are denoted in Fig. 6 by triangles. There are five objects, Nos. 20, 48, 120, 169 and 198 which are so bright to cause saturation in the DENIS observation and rejection from the DENIS catalogue. From their locations in Fig. 6, sources Nos. 48, 169 and 198 may be nearby RGB star or an intermediate AGB star with relatively thin circumstellar envelope; sources Nos. 20 and 120 are redder and brighter, thus may be luminous AGB stars with thick circumstellar envelope.

The non-detection of the other sources is due to their faintness in the DENIS bands. The faint 15 μm ISO sources with [15] > 6.0 not detected in DENIS are partly mixed with those detected in the K_S-band and not detected in the J-band in Fig. 6 that were suspected to be candidates for YSOs, again due to their red color and low luminosity. Their non-association with DENIS can be accounted for by heavy absorption and coldness

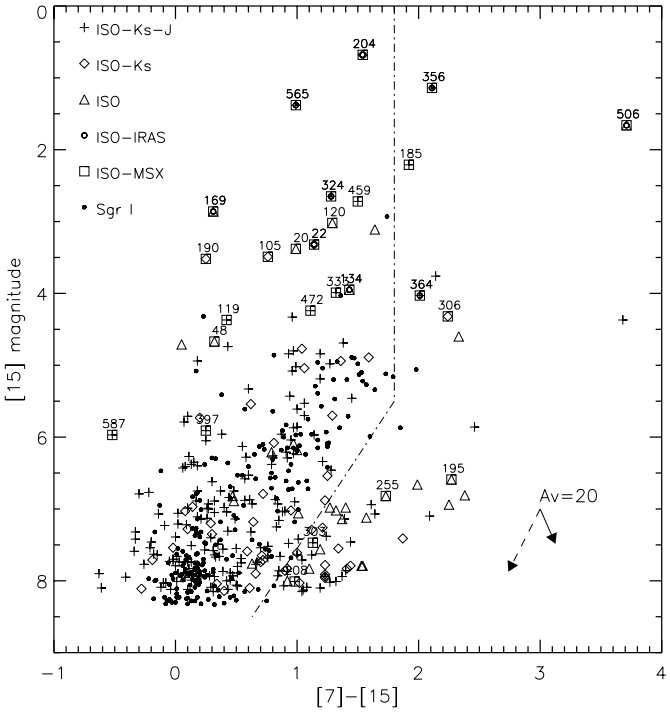

Fig. 6. Color-magnitude diagram [7]–[15] vs. [15]without dereddening. The sources in the field FC–01863+00035 are denoted by crosses for associations with both J and K_S bands, by diamonds for associations only with the K_S-band and triangles for non-associations with DENIS. Those identified with the IRAS PSC objects are circled, and with MSX point source catalogue are squared. The objects identified with IRAS and/or MSX catalogues are numbered at the top by their sequence in the ISOGAL field catalogue. (The sources in the SgrI field are decoded by dots.) Extinction arrow is displayed at the lower-right corner for $A_V = 20$ mag, with the two determinations of A_{15} of Fig. 4 (right). Dot-dashed line represent the approximate borders between YSOs and late-type stars, suggested by Felli et al. (2000).

of circumstellar disk of YSOs, plus possibly interstellar extinction. However, their nature needs confirmation since most of the reddest and weakest sources in Fig. 6 ([7]–[15]>1.5) have at least one ISOGAL magnitude of poor quality (as well as the sources with $(K_S\text{-}[7])_0 \geq 2.0$ and $[7]_0 \leq 7.5$ in Fig. 7).

The sources detected only in the LW2 band are mostly faint with [7] < 8.0 (see Fig.2). If they are not artifacts, the non-detection in LW3 can be understood by the lower sensitivity of ISOCAM in the LW3 band than in the LW2 band, the incompleteness in the LW3 band to faint objects, and because the spectral energy distribution (SED) of the objects do not rise steeply from 7 μm to 15 μm. As the DENIS survey is almost complete to $K_S = 11.0$ mag, their color index K_S–[7] would be greater than 2.0 and possibly very large, i.e. $A_V > 30$ since the limiting [7] magnitude is taken to be 9.38. They must be distant, for example, further than the near side of the Norma arm. On the other hand, the objects were detected in LW2 at such large distance, which means they must be bright in LW2. The study of ISOGAL variables in the Galactic bulge showed that the AGB variables are distinguishable from other M-type giants by their high 7 μm luminosities (Schultheis et al. 2000; Schultheis & Glass 2001). So they are possibly AGB variables.

The sources detected only in LW3 are mostly fainter than magnitude 7.0. The incompleteness of the ISOGAL survey in LW2 to faint objects can account for part of the non-detection in LW2. However, the reality of weak unassociated LW3 sources should be confirmed. There may be some real sources that are candidates for YSOs. The low temperature of YSOs peaks their radiation in middle and even far infrared. The non-detection in shorter wavelengths can be understood by their weak emission in these bands. If they were RGB or AGB stars, the higher sensitivity of ISOCAM in LW2 should bring them to the detection limit in LW2. More observation of these sources would reveal their identity.

4.4. Sources identified in IRAS or MSX PSC

Although the IRAS photometric results of these faint sources are mostly uncertain at 60 and 100 μm (Table 4), the difference in the SED in the IRAS four bands between AGB stars and YSOs is generally clear. The YSOs rise more steeply in SED from 12 to 100 micron than AGB stars. According to the IRAS colors, there are three YSO candidates #134, #364 and possibly #506 (or IRAS16464-4359, IRAS16469-4348 and IRAS16472-4351) which have steep SED in the IRAS bands. A further support comes from the ISOGAL imaging, i.e. around the first two YSO candidates extended nebulae are clearly visible in the ISOCAM images in both LW2 and LW3 bands (see also Fig. 1). In addition, sources #364 and #506 lie in a region of the [7]–[15]/[15] diagram assigned to YSOs by Felli et al. (2000), and #134 lies slightly left of the borderline between YSOs and late-type stars and it is still acceptable to be a YSO. However, for #506, the MSX color D–E appears anomalously blue for a YSO.

All the other IRAS objects, except #169, are probably AGB stars with high mass loss rate. The first criterion is that their IRAS colors mimic such stars. Moreover, the IRAS variability indexes of #204 and #565 are 83 and 79 respectively, which seems to point out to variable late-type stars. One object #22 (IRAS 16459-4354) is an OH maser star (Sevenster et al. 1997). All are in the region where the large-amplitude long-period variables are found in Fig. 6. The location in Fig. 6 of these objects whose AGB nature is confirmed by IRAS fluxes supports the consistency of the borderline between AGB stars and YSOs proposed by Felli et al. (2000). These ISO-IRAS objects are bright sources in the ISOGAL catalogue since the ISOGAL sensitivity is much higher than IRAS. However, because they have large A_V and are either AGB stars with high mass loss rate or YSOs embedded in cold circumstellar envelope, they also exhibit very red colors in the DENIS bands. In spite of their brightness in LW2 and LW3 bands, no IRAS object was bright enough to be detectable in the I-band by DENIS, except one, #169, whose non-detection by DENIS was caused by saturation other than by faintness.

The ISOGAL objects were also cross-identified with the MSX point source catalogue available at `http://www.ipac.caltech.edu/ipac/msx/msx.html`. The MSX (Midcourse Space eXperiment) surveyed the entire Galactic plane between +4.5° and –4.5° at 4.3 μm (band B),

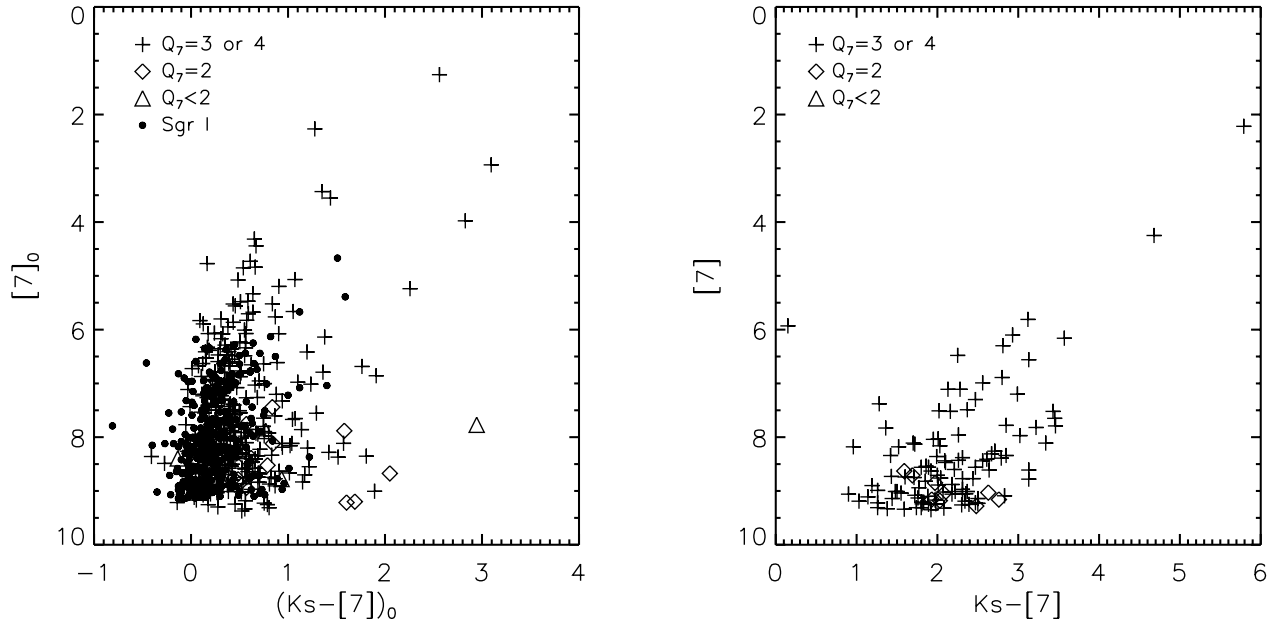

Fig. 7. Color-magnitude diagram K_S–[7] vs. [7]. Left panel: Sources detected in both J and K_S bands and thus corrected for interstellar extinction. The objects with good, moderate and poor quality flags at 7 μm are decoded by pluses, diamonds and triangles respectively. The Sgr I objects are again represented by dots and corrected for the extinction by 0.2 mag in the K_S-band. Right panel: Sources not detected in the J-band and thus not corrected for interstellar extinction. The pluses, diamonds and triangles decode the sources with good, moderate and poor quality flags at 7 μm.

8.3 μm (band A), 12.1 μm (band C), 14.6 μm (band D) and 21.3 μm (band E) (Egan et al. 1996; Price et al. 2001). The FC–01863+00035 ISOGAL field was in the MSX observing area. In order to cross identify the ISOGAL sources with the MSX objects, the search radius was set to 10″ which is about 4σ position uncertainty of MSX (Cohen et al. 2000). The brightness of the ISOGAL objects to be associated with MSX is also limited to those with [7] < 7.0 since the MSX SPIRIT III detector was much less sensitive than ISOCAM, so that the possibility of spurious chance associations is quite negligible. Twenty-five ISOGAL objects (4%) are found to have counterpart in the MSX PSC catalogue and they are all shown in Fig. 6. The MSX results of the objects associated with IRAS PSC are listed in Table 4. Most of them, with [15] < 6.0 and 0.5 < [7]–[15] < 1.6, have MSX color indexes like luminous mass-losing AGB stars, more or less distant. Three of them (#306 (not in Table 4), #364 and #506, plus #134) are probably YSOs from their color [7]–[15] > 1.8 and their MSX colors; they could be nearby or massive since they are all brighter than 5 mag at [15].

A table with such data about all ISOGAL-MSX associations is available at CDS (Table 5). At least six blue sources with [7]–[15] < 0.4 (#48, #119, #169, #190, #397 and #587, see Fig. 6) should be relatively nearby stars with little circumstellar dust, either RGB, or early AGB, or main sequence stars.

5. Conclusion

The combination of 7 and 15 μm ISOGAL data with near-infrared DENIS data is powerful to trace the extinction and Galactic structures on the lines of sight of ISOGAL fields in

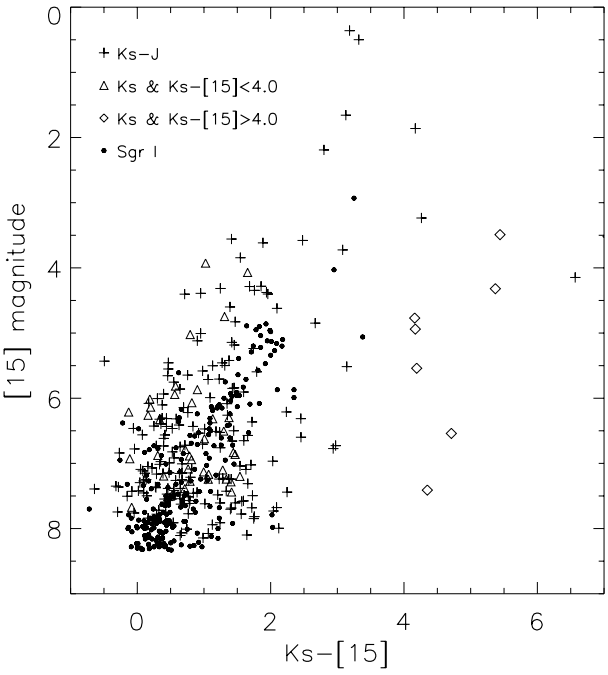

Fig. 8. Color-magnitude diagram K_S–[15] vs. [15]. The sources detected in both J and K_S bands (crosses) are corrected for interstellar extinction according to their J–K_S values. Those not detected in the J-band with K_S–[15] < 4.0 (triangles) are corrected for interstellar extinction according to their K_S–[7] values, and their K_S–[15] and [15] are corrected for interstellar extinction. The objects that were not detected in the J-band and K_S–[15] > 4.0 (diamonds) are not corrected for interstellar extinction and their observed colors and magnitudes are shown.

Table 4. ISOGAL sources cross-identified in the IRAS PSC catalogue. These sources, except #169, are too faint to be detected in the DENIS *I*-band. Their DENIS magnitudes, ISOGAL magnitudes and flux densities, IRAS flux densities at 12, 25, 60 and 100 μm, and MSX flux densities in band *A* (8 μm), *C* (12 μm), *D* (15 μm) and *E* (21 μm) are listed in order.

ISO	IRAS PSC	*J*	K_S	[7]		[15]		12	25	60	100	*A*	*C*	*D*	*E*	Type
		mag	mag	mag	Jy	mag	Jy	Jy	Jy	Jy	Jy	Jy	Jy	Jy	Jy	
22	16459-4354	–	10.9	4.4	1.4	3.3	0.9	–	2.1	–	–	0.5	–	1.2	–	AGB
134	16464-4359	–	–	5.3	0.6	3.9	0.5	–	9.0	199.0	–	1.4	–	1.0	3.3	YSO
169	16465-4344	Saturation		3.1	4.8	2.8	1.4	2.0	–	–	–	2.4	1.6	1.2	–	?
204	16466-4353	–	8.0	2.2	11.5	0.6	11.0	4.3	6.3	–	–	6.4	7.6	8.2	7.1	AGB
324	16468-4349	15.5	8.9	3.9	2.3	2.6	1.8	–	1.3	–	–	0.6	1.1	1.2	–	AGB
356	16469-4356	12.9	6.4	3.2	4.4	1.1	7.2	5.2	4.7	–	–	3.0	6.0	5.8	4.0	AGB
364	16469-4348	12.0	7.7	6.0	0.3	4.0	0.5	–	1.6	64.7	236.5	0.4	–	–	2.4	YSO
506	16472-4351	–	–	5.3	0.6	1.6	4.4	3.4	8.4	–	–	–	2.0	3.6	4.7	YSO?
565	16475-4349	14.3	7.0	2.3	10.0	1.3	5.8	5.6	7.3	–	–	3.8	5.0	5.5	5.4	AGB

the inner Galactic disk. Our detailed analysis of the good quality ISOGAL-DENIS data of the field FC–01863+00035 has firstly allowed to derive a reasonably accurate value of the extinction at 7 μm through $A_{K_S} - A_7 = 0.35(A_J - A_{K_S})$ which yields $A_7/A_V \sim 0.03$ from the near-IR extinction values of van de Hulst–Glass (Glass 1999). One can thus use the value of the color K_S–[7] to determine the very large interstellar extinction on the lines of sight of the ISOGAL sources without too much circumstellar dust, in the range of $A_V \sim 25$–45 where the DENIS data alone fail because of non-detection in the *J*-band. The preliminary comparison with CO and HI data confirms that most of the interstellar extinction comes from the large molecular clouds in the Centaurus arm which produces the bulk of the CO and HI emission. For sources with very large extinction, future studies with higher-resolution CO data should help to distinguish whether the excess of extinction mainly comes from a condensation in this cloud or from additional dust layers farther out.

The combination of the ISOGAL and DENIS data and the knowledge of the interstellar extinction allow an approximate determination of the nature of most of the ISOGAL sources. As in other ISOGAL fields, the bulk of ISOGAL sources are AGB stars with weak mass-loss and bright RGB stars, with some high mass-loss AGB stars and of bluer and less luminous foreground stars, together with a few YSOs. The combination with MSX and IRAS data helps to identify more precisely the brightest and reddest sources and to find the most interesting ones for follow-up studies. The values of the colors $(K_S–[15])_0$ and [7]–[15] could provide reasonably accurate estimates of the mass-loss rates of AGB stars (e.g. Ojha et al. 2003). The information about the extinction structure on the line of sight may bring some information on the distance of ISOGAL sources in the Galactic disk. But the distances are still much too uncertain to allow accurate estimates of the luminosities, and, hence, to elaborate, e.g., on the age of the AGB populations. The main differences between this disk field and Baade's Window are that there is a larger proportion of relatively nearby objects, and that there is a branch of a few YSO candidates. They either have a redder color index [7] – [15] > 1.6 or were detected only in the LW3 band. However, further observations are needed to confirm their nature.

There are obviously many possible extensions of such a case study of an ISOGAL field: systematic similar analysis of the extinction in all other ISOGAL fields; extended studies of stellar populations in various disk fields which is in progress (Felli et al. 2002); detailed combined studies with better CO data, and with continuum mm/submm emission of molecular clouds; systematic analysis of mass-loss of AGB stars of the inner Galactic disk; identification of lists of particular interesting sources for spectroscopic follow-up studies, in particular in the mid-IR with SIRTF, in the near-IR with various ground telescopes, and in the visible for low–extinction sources; more sophisticated analysis with multi-wavelength data at high angular resolution from the SIRTF/GLIMPSE legacy program and from wide-field near-IR cameras.

Acknowledgements. B.W. Jiang thanks NKBRSF G19990754 and the support from CAS and CNRS, and Dr. Aigen Li for useful discussion. We particularly thank M. Schultheis, F. Sévre and T. August for their help. We thank Dr. G. Gilmore for his helpful referee's comments and suggestions. S. Ganesh, G. Simon and A. Omont acknowledge support from Project N. 1910-1 of the Indo–French collaboration CEFIPRA/IFCPAR.

References

Bachiller, R., & Cernicharo, J. 1986, A&A 166, 283
Bertelli, G., Bressan, A., Chiosi, C., Fagotto, F., & Nasi, E. 1994, A&A, 106, 275
Bloemen, J., Deul, E., & Thaddeus, P. 1990, A&A, 233, 437
Bontemps, S., André, P., Kaas, A., et al. 2001, A&A, 372, 173
Bronfman, L., Alvarez, H., Cohen, R. S., & Thaddeus, P. 1989, ApJS, 71, 481
Cardell, J., Clayton, G., & Mathis, J. 1989, ApJ, 345, 245
Cesarsky, C., Abergel, A., Agnesse, P., et al. 1996, A&A, 315, L32
Cohen, M., Hammersley, P., & Egan, M. 2000, AJ, 120, 3362
Combes, F. 1991, ARA&A, 29, 195
Dame, T., Ungerechts, R., Cohen, R., et al. 1987, ApJ, 322, 706
Dame, T., Hartmann, D., & Thaddeus, P. 2001, ApJ, 547, 792
Draine, B., & Lee, H. 1984, ApJ, 285, 89
Egan, M., & Price, S. 1996, AJ, 112, 2862
Epchtein, N., De Batz, B., Capoani, L., et al. 1997, Messenger 87, 27

Felli, M., Comoretto, G., Testi, L., Omont, A., & Schuller, F. 2000, A&A, 362, 199
Felli, M., Testi, L., Schuller, F., & Omont, A. 2002, A&A, 392, 971
Glass, I. 1999, Handbook of Infrared Astronomy (Cambridge Univ. Press)
Glass, I., Ganesh, S., Alard, C., et al. 1999, MNRAS, 308, 127
Harjunpaa, P., & Mattila, K. 1996, A&A, 305, 920
Hennebelle, P., Pérault, M., Teyssier, D., & Ganesh, S. 2001, A&A, 365, 598
Lopez-Corredoira, M., Hammersley, P., Garzon, F., et al. 2001, A&A, 373, 139
Lutz, D. 1999, in The Universe as seen by ISO, ed. P. Cox, & M. Kessler, ESA-SP427, 623
Mathis, J. 1990, ARA&A, 28, 37
Neckel, Th., & Klare, G. 1980, A&AS, 42, 251
Ojha, D., Omont A., Simon, G., et al. 2003, A&A, submitted
Omont, A., Ganesh, S., Alard, C., et al. 1999, A&A, 348, 755
Omont, A., Gilmore, G., Alard, C., et al. 2003, A&A, submitted
Ott, S., Abergel, A., Altieri, B., et al. 1997, in Astronomical Data Analysis Software and Systems VI, ed. G. Hunt, & H. Payne, ASP Conf. Ser., 125, 34 (San Franciso: ASP)
Pérault, M., Omont, A., Simon, G., et al. 1996, A&A, 315, L165
Price, S. D., Egan, M. P., Carey, S. J., et al. 2001, AJ, 121, 2819
Rieke, G., Rieke, M., & Paul, A. 1989, ApJ 336, 752
Schuller, F., Ganesh, S., Messineo, M., et al. 2003, A&A, submitted
Schultheis, M., Ganesh, S., Simon, G., et al. 1999, A&A, 349, L69
Schultheis, M., Ganesh, S., Glass, I., et al. 2000, A&A, 362, 215
Schultheis, M., & Glass, I. 2001, MNRAS, 327, 1193
Sevenster, M., Chapman, J., Habing, H., Killeen, N., & Lindqvist, M. 1997, A&AS, 124, 509
van de Hulst, H. C. 1946, Rech. Astron. Obs. Utrecht, 11, 1
van Loon, J. T., Gilmore, G., Omont, A., et al. 2003, MNRAS, 338, 857
Wainscoat, R., Cohen, M., Volk, K., Walker, H., & Schwartz, D. 1992, ApJS, 83, 146